ADVANCED MATERIALS
www.advmat.de

Preparation of Macroscopic Block-Copolymer-Based Gyroidal Mesoscale Single Crystals by Solvent Evaporation

*Ethan M. Susca, Peter A. Beaucage, R. Paxton Thedford, Andrej Singer, Sol M. Gruner, Lara A. Estroff, and Ulrich Wiesner**

Properties arising from ordered periodic mesostructures are often obscured by small, randomly oriented domains and grain boundaries. Bulk macroscopic single crystals with mesoscale periodicity are needed to establish fundamental structure–property correlations for materials ordered at this length scale (10–100 nm). A solvent-evaporation-induced crystallization method providing access to large (millimeter to centimeter) single-crystal mesostructures, specifically bicontinuous gyroids, in thick films (>100 µm) derived from block copolymers is reported. After in-depth crystallographic characterization of single-crystal block copolymer–preceramic nanocomposite films, the structures are converted into mesoporous ceramic monoliths, with retention of mesoscale crystallinity. When fractured, these monoliths display single-crystal-like cleavage along mesoscale facets. The method can prepare macroscopic bulk single crystals with other block copolymer systems, suggesting that the method is broadly applicable to block copolymer materials assembled by solvent evaporation. It is expected that such bulk single crystals will enable fundamental understanding and control of emergent mesostructure-based properties in block-copolymer-directed metal, semiconductor, and superconductor materials.

Dr. E. M. Susca,[+] Dr. P. A. Beaucage,[++] R. P. Thedford, Prof. A. Singer, Prof. L. A. Estroff, Prof. U. Wiesner
Department of Materials Science and Engineering
Cornell University
Ithaca, NY 14853, USA
E-mail: ubw1@cornell.edu

R. P. Thedford
Robert Frederick Smith School of Chemical and Biomolecular Engineering
Cornell University
Ithaca, NY 14853, USA

Prof. S. M. Gruner
Department of Physics
Cornell University
Ithaca, NY 14853, USA

Prof. S. M. Gruner, Prof. L. A. Estroff
Kavli Institute at Cornell for Nanoscale Science
Ithaca, NY 14853, USA

The ORCID identification number(s) for the author(s) of this article can be found under https://doi.org/10.1002/adma.201902565.

[+]Present address: Department of Chemical Engineering and Materials, University of California Santa Barbara, Santa Barbara, CA 93106, USA

[++]Present address: Material Measurement Laboratory, National Institute of Standards and Technology, Gaithersburg, MD 20899, USA

DOI: 10.1002/adma.201902565

Single crystals are materials with periodic structure that extends across macroscopic distances as a coherent lattice free of grain boundaries. By isolating and studying their properties, bulk single crystals have revolutionized our fundamental understanding of materials from semiconductors to biomacromolecules, fueling innovations from microelectronic devices to pharmaceutical compounds. In contrast, our understanding of many mesostructured materials is still in its infancy in part due to the lack of available single crystals.[1,2] Block copolymer (BCP) self-assembly is a promising method to prepare periodic 10–100 nm structures[3,4] with coherent orientation over macroscopic lengths.[5–7]

There have been notable successes in the preparation of single crystal BCP mesostructures, in particular confined to two dimensions in thin films. By limiting film thickness, crystal growth techniques employing solvent and thermal gradients or electric, magnetic, and mechanical field-aligning techniques have generated centimeter-sized structures with coherent orientation in two dimensions.[8,9] Furthermore, self-assembled BCP thin films may self-orient based on the nature of the 2D boundary conditions by preferential wetting or epitaxy to underlying substrate patterns.[2,10,11] These interactions, however, typically die off after a few unit cells away from the substrate rendering this approach ineffective for thick/bulk films.

While self-assembly of BCP monodomains in thin films has been widely investigated, the formation of bulk mesophase single crystals is usually limited to anisotropic phases (e.g., cylinders or lamellae), which can be aligned by a single large gradient or field under carefully controlled conditions.[5,12,13] In contrast, bulk single crystal materials from isotropic 3D periodic BCP network structures, like the cubic gyroid lattice, are much more difficult to achieve.[14] Recently, interest in preparing macroscopic single crystals of such 3D periodic BCP gyroid networks has substantially increased due to prediction or experimental evidence of emergent properties including negative refraction, flux pinning in superconductors, or topologically protected surface states (i.e., Weyl fermions).[15–17] Single crystal gyroid materials with long-range crystallographic orientation would enable fundamental understanding and control of angle-dependent properties.[18,19]

This work uses two large triblock terpolymers—poly(isoprene-*b*-styrene-*b*-dimethylaminoethylmethacrylate)

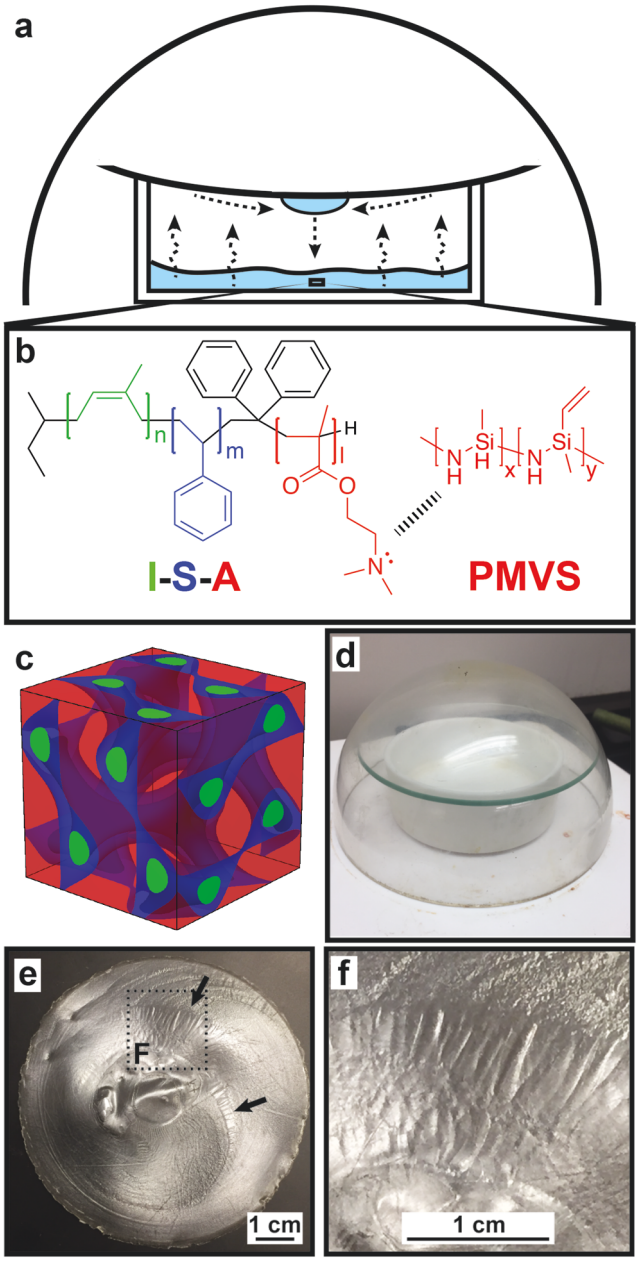

Figure 1. Schematic of self-assembly apparatus and double gyroid materials. a) Cross-sectional schematic of a dome enclosing an evaporating dish with a watch glass lid. Arrows show transport of toluene solvent within dish: vapor condenses on watch glass and is drawn to center before returning to solution. b) Chemical structures and hydrogen bonding of triblock terpolymer (ISA) and preceramic (PMVS). c) Schematic of double gyroid mesostructure with colors matching components in (b). d) Photograph of setup shown schematically in (a). e) Dry, circular disk-like self-assembled thick film with arrows showing elongated single crystal regions distinguishable by eye. f) Inset of region highlighted in (e) showing high aspect ratio single crystal grains.

(PI-*b*-PS-*b*-PDMAEMA or simply ISA, **Figure 1**b)—to generate bulk single crystals distinguishable by eye (Figure 1) through an evaporation-induced self-assembly (EISA) route. Polymers with total molar mass of 71 or 96 kg mol^{-1} (ISA71, ISA96)—with block volume fractions I/S/A of 18/32/50 ± 1 vol% and polydispersity index 1.09—are used to structure-direct a preceramic polymer, poly(methyl vinyl silazane) (PMVS), into double gyroid (Q^{230}, $Ia\bar{3}d$) mesostructured phases. Single crystalline mesostructures spanning 7 mm^2 are assembled in 7–10 days from the larger terpolymer, while the smaller terpolymer forms up to 14 mm^2 large crystals in 24 days in samples 100–300 µm in thickness. These gyroidal BCP single crystal domain volumes are over three orders of magnitude larger than previously reported.[20–23] Freestanding films could be converted to mesoporous silicon (oxy)nitride monoliths with double gyroid pore geometry.[24,25] These porous structures have potential as templates for functional materials that are difficult to directly coassemble with BCPs.[26–28]

The preparation and characterization of self-assembled thick films consisting of large mesoscale crystalline domains are described in Figure 1 (preparation), **Figure 2** (characterization), and additionally in the Experimental Section. The key experimental variables for obtaining large crystalline domains are achieving slow solvent evaporation, coupled with solvent recirculation. To achieve these conditions, a watch glass is placed above the solution of polymer and PMVS (or polymers only, vide infra) as an initial barrier to solvent evaporation, with its convex side pointing down. Introduction of this watch glass to a typical solvent evaporation setup yields crystalline domains at least three orders of magnitude larger than without it. A hemispherical dome is additionally placed over both the watch glass and dish to further slow solvent evaporation (Figure 1a,d). As the solvent evaporates, hydrogen bonding between the PDMAEMA block and PMVS (Figure 1b) drives the coassembly of ISA and PMVS into the majority "matrix" domain (Figure 1c, red domain) of the double gyroid mesostructure.[29] This matrix divides two interpenetrating minority PI/PS core/shell single gyroid strut networks (Figure 1c, green/blue PI/PS domains).

Recirculation of the solvent, toluene, was observed within the modified evaporative self-assembly setup. Specifically, toluene was directed toward the center of the circular dish by its vapor condensing into droplets along the convex (lower) side of the watch glass. These droplets gradually moved toward the center of the lid, due to gravity and the shape of the glass, where they merged into larger droplets that ultimately fell back into the center of the solvated polymer mixture. During this recirculation process, toluene was also slowly removed because the setup was kept unsealed. Dried films were flat and circular with regions of smooth, high aspect ratio features arranged in an arc (Figure 1e, arrows; Figure 1f). When the watch glass was positioned such that its convex side was up, these macroscopic high aspect ratio features did not form, suggesting that recirculation of solvent to the center of the dish plays a key role in crystal growth. This work shows these features diffract as single mesoscale crystals over areas as large as 14 mm^2 and can be isolated for further study.

Small-angle X-ray scattering (SAXS) was used to characterize mesostructure by spatially mapping 2 cm^2 of each sample with a 100 × 100 µm^2 collimated beam in steps of 100 µm along directions orthogonal to the beam (Figure 2a). A photograph of a circular section of the as-made ISA96/PMVS nanocomposite sample is shown in Figure 2b. All samples were oriented with their lower edge closest to the center of the disk-like films, while the upper edge was closest to the disk rim.

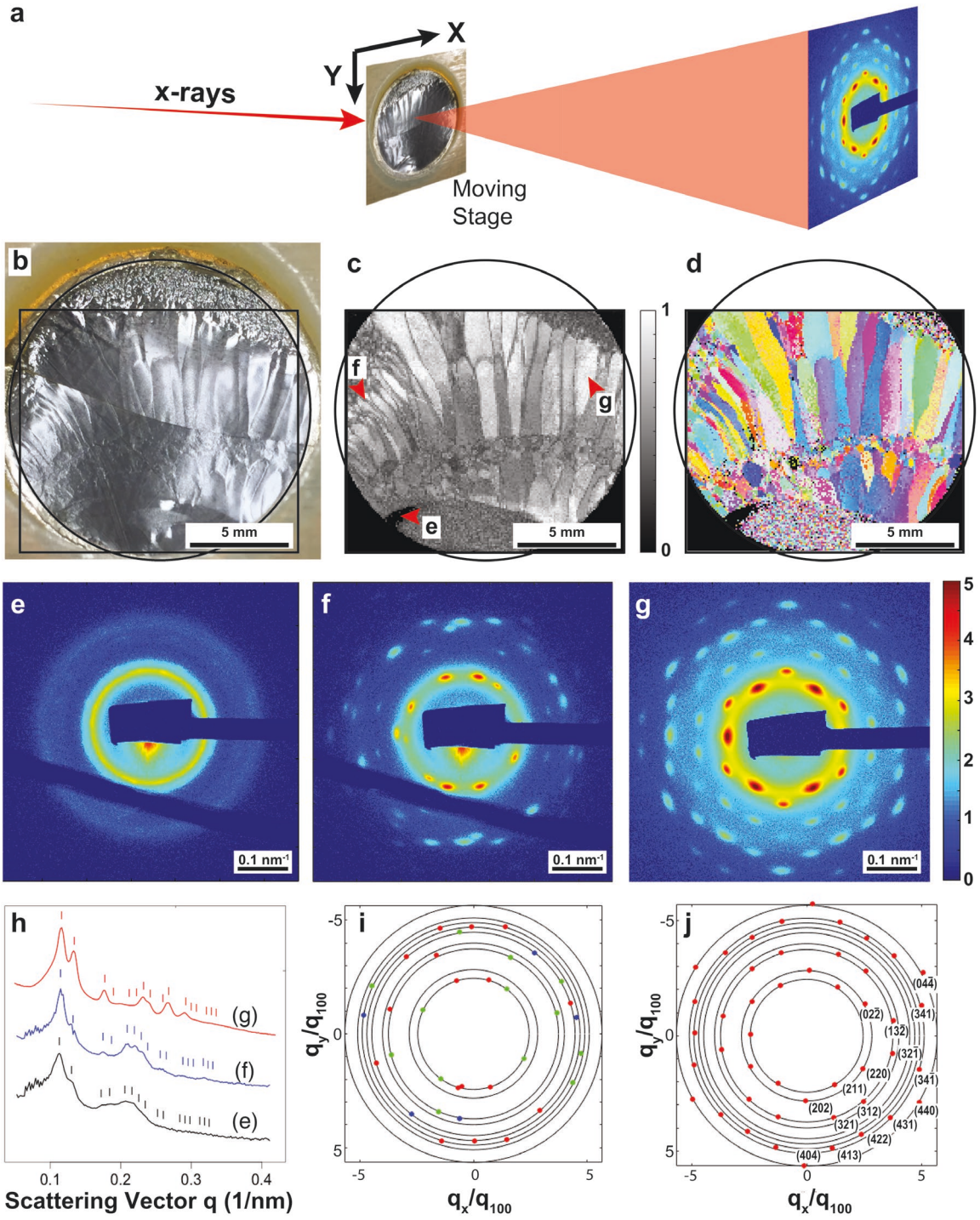

Figure 2. Small-angle X-ray scattering (SAXS) setup and analysis for a nanocomposite containing 96 kg mol^{-1} structure-directing polymer, ISA96. a) 2D SAXS patterns were collected as samples moved orthogonally to the beam. Each 2D SAXS pattern forms one pixel of final maps. b) Photo of mounted sample cut using a circle punch out of the larger film with black rectangular frame indicating area scanned with X-rays. c) A map of the fraction of identified Bragg reflections accounted for by calculated diffraction patterns. d) Orientation map where colors denote gyroid orientation relative to lab horizontal *X*-axis in (a) (see also Figure S1 in the Supporting Information). e–g) Representative SAXS patterns with log scale colors from locations as indicated in (c), exhibiting polycrystalline (e), multi-(three) crystalline (f), and single crystal (g) behavior. Diagonal bars across bottom are shadows from photodiode wire. h) Radially integrated patterns from (e–g) with expected polycrystalline gyroid reflections marked. Systematic absences from the integrated single crystalline sample (g) are consistent with the assigned crystal orientation. i) Indexed peak positions for (f) from three different microdomains. j) Indexed peak positions for (g) corresponding to the [$\bar{1}$11] zone axis orientation. For clarity, only one third of the peaks have indices labeled.

An algorithm extracted gyroid crystal orientation for tens of thousands of SAXS patterns by comparing measured Bragg reflection positions with calculated diffraction patterns.[20,21] Figure 2c shows a grayscale map of a simple figure of merit: the fraction of identified Bragg reflections that can be fitted to a calculated single crystal diffraction pattern. Each bright region corresponds to a single crystal orientation (see also Figure S2 in the Supporting Information) and grain boundaries appear darker. The map reproduces the mm^2-sized domains that can be identified by eye (Figure 2b), where domains were found to correspond to individual gyroid mesostructured single crystals. Figure 2d is a color map showing the orientation of gyroid single crystal regions relative to the horizontal lab frame direction (Figure S1, Supporting Information). The many disparate colors indicate no preferential crystal orientation in this direction.

2D SAXS patterns from regions indicated with red arrows in Figure 2c are shown in Figure 2e–g with their radially integrated patterns depicted in Figure 2h. Figure 2e reveals a highly polycrystalline pattern in which the scattering produces rings since crystallites are much smaller than the X-ray probe (100×100 μm^2). The scattering pattern in Figure 2f highlights a sample area that is multicrystalline with a few grains within the X-ray probe volume. Iteratively employing the peak-fitting algorithm suggests three crystallites contribute to this diffraction pattern (Figure 2i). Figure 2g is produced from a single crystallographic zone in which all reflections can be accounted for by a single calculated diffraction pattern (zone axis = $[\bar{1}11]$) shown with one third of the reflections indexed in Figure 2j. This single crystal region spans 4.7 mm^2.

Macroscopic double gyroid single crystals prepared in this study had high aspect ratios, suggesting a possible preferential crystal growth axis along the radial direction of the circular evaporation dish (lab frame *Y* axis, Figure 2a). Plotting the crystallographic orientation on an inverse pole figure, however, shows a relatively homogenous spread of orientations relative to this direction (**Figure 3**a, right). Crystallographic orientation maps corroborate the lack of preferred orientation along this axis, as demonstrated by the randomly colored map denoting the observed crystallographic directions (Figure 3a, left).

In contrast, the orientation maps and inverse pole figures along the beam direction (normal to film, Figure 2a) showed a clear out-of-plane crystallographic texture (Figures 3b; Figure S1, Supporting Information). The largest bulk single crystals were assembled from ISA71-directed blend and spanned record areas of 10 and 14 mm^2. These crystals had mostly [522] out-of-plane orientation, as confirmed by direct inspection of 2D SAXS patterns (Figure S2, Supporting Information). [522] is among several observed out-of-plane orientations less than 6° separated from [211], depicted by magenta colors in the orientation maps (Figure 3c). Since the error associated with orientation fitting is ±5° (Figure S3, Supporting Information), we conclude that the set of orientations near [211] are preferred out-of-plane directions.

Williamson–Hall (WH) analysis was performed on ISA96/PMVS blend to determine the degree of long-range order in the single crystals.[30,31] The analysis assumes a mosaic block model where lattice distortion, misorientation, and coherent scattering domain size contribute independently to Bragg reflection broadening. The model employs a linear relationship (Equation (1)) between reflection peak widths ($w_{\phi,q}$) and their scattering vector magnitude ($|q|$) for reflection profiles following Lorentz distributions (Figure S4, Supporting Information). The slope of this relationship yields misorientation (g_ϕ) or lattice distortion (g_q) parameters from peak width analysis in the azimuthal (w_ϕ) or scattering (w_q) directions, respectively. The extrapolated intercept is inversely related to the length of a perfectly coherent scattering domain, L_{CSD}, which can be measured up to the coherence length of the X-ray source (2.5 μm, see the Supporting Information).

$$w_{\Phi,q}(|q|) = g_{\Phi,q}|q| + \frac{2\pi}{L_{CSD_{\Phi,q}}} \quad (1)$$

For WH analysis, the sample was oriented with the X-ray beam axis (lab frame *Z*) along the [111] gyroid axis (Figure 3b/e, dark blue), so that statistically significant mean peak width and standard error could be calculated from the five or six reflections available at each scattering vector magnitude, $|q|$. A single crystal region (Figure 3b, black box) is enlarged in Figure 3e with three representative SAXS patterns (Figure 3e,i–iii) taken at three locations (i, ii, iii) along a straight line through the 5 mm long grain (from bottom to top) annotated in Figure 3f–h. Figure 3f shows Bragg peak full-width at half-maximum (FWHM) in the azimuthal (ϕ) direction as a function of scattering vector magnitude. For each location, linear regressions to Equation (1) were used to evaluate how misorientation, g_ϕ (Figure 3g), lattice distortion, g_q (Figure 3h), and coherent scattering domain lengths ($L_{CSD\phi,q}$) vary along the length of the grain.

Here, g_ϕ decays from 9° and stabilizes at 4° when measured along the line-scan toward the sample edge (Figure 3e,g). The associated coherently scattering domain size, L_{CSD}, varies from about 2 to about 3 μm (Figure S4, Supporting Information), consistent with the upper limit defined by the coherence length of the X-ray source in this experiment. Therefore, our results suggest a macroscopic mosaic single crystal consisting of defect-free domain sizes of at least 2.5 μm, with 4°–9° average misorientation over macroscopic (mm) dimensions. WH analysis performed along the scattering direction, *q*, yielded a lattice distortion parameter, g_q, decaying from 8% to 4% along the line-scan, with associated coherent scattering domain sizes near the X-ray coherence length limit (Figure S4, Supporting Information).

The large, single crystal gyroid domains grown in this work share two interesting characteristics, which provide possible clues to their growth mechanism: 1) the WH analysis shows that the crystal perfection, along with crystal size, increases moving toward the edge of the sample and 2) the crystals display a preferred out-of-plane [211] orientation. In thin films, often only a single-field-gradient, or growth front is needed to generate single crystals spanning the two macroscopic, in-plane, film dimensions.[32–35] In this case, block/substrate wetting effects can wholly determine film normal orientation since thin films are usually less than ten unit cells thick. This geometry leaves only one in-plane direction (a single degree of freedom) needed to specify the global crystallographic orientation. In bulk materials, however, a 2D boundary condition is

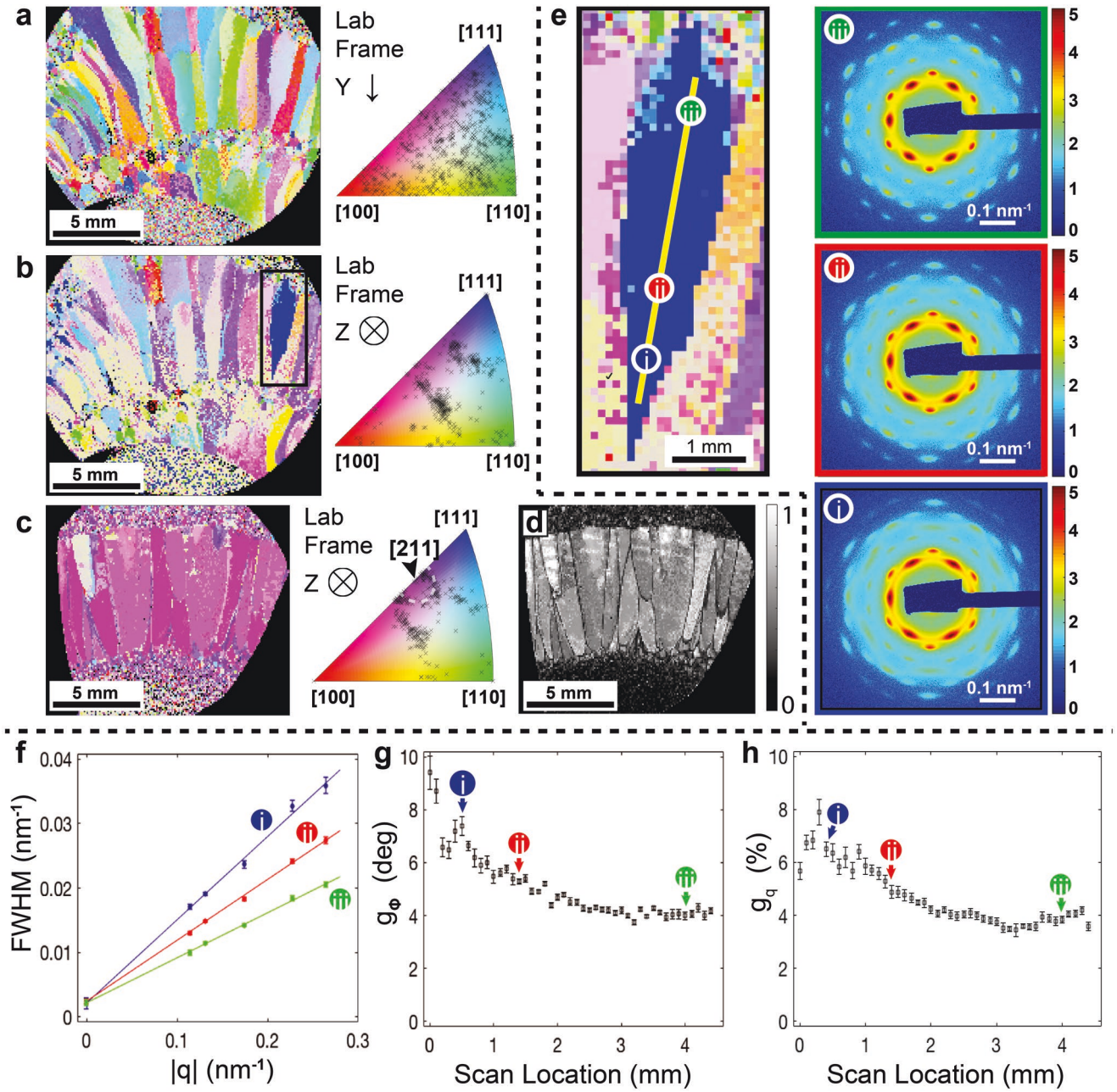

Figure 3. Orientation maps, inverse pole figures, and Williamson–Hall (WH) analysis—see Figure S4 in the Supporting Information for additional details. a,b) Orientation maps and corresponding inverse pole figures of a film from ISA96/PMVS blend showing crystallographic direction expressed along the *Y* (a) and film normal (b) axes. c) Orientation map and inverse pole figure relative to the film normal for ISA71/PMVS blend. The inverse pole figure displays orientations near the [211] direction (black arrow). A white dashed line encloses orientations ±5° from [211], the error associated with the orientation fit algorithm (see Figure S3 in the Supporting Information). d) Figure of merit map of the fraction of identified reflections accounted for by the best-fitting calculated pattern revealing record grains of 14 and 10 mm^2 sizes (see Figure S2 in the Supporting Information). e) Region inset in (b) used for single-crystal WH analysis with sample 2D diffraction patterns (e,i–iii) (log scale colors) from locations along a line scan shown in (e). Figure 2g is a fourth diffraction pattern from a different location within the same crystal. f) Sample WH linear regression plots for azimuthal peak widths from patterns shown in (e,i–iii). g) Misorientation parameter and h) lattice distortion (strain) measured along line scan.

unlikely to completely determine the orientation in the direction perpendicular to the bounding plane because bulk materials are thousands of unit cells thick and, therefore, two orthogonal fields or gradients are often needed to control orientation along a minimum of two directions. Evaporation front pinning, meniscus flow, and strong solvent flows have all been suggested as possible orthogonal fields to help promote large 3D mesophase crystal formation.[36–38]

In this system, there is a continuous recirculation of solvent to the center of the evaporation dish during self-assembly,

resulting in a polymer concentration profile that changes with each solvent droplet returning to solution. On average, this recirculation creates a higher concentration of polymer near the perimeter of the dish. If this average concentration gradient is responsible for the observed crystal growth patterns, crystals ought to nucleate near the perimeter (at high polymer concentration) and grow inward toward the center. We speculate that the overall polymer concentration gradient promotes growth inward that is disrupted by toluene droplets falling to the center from the watch glass cover. The pure toluene droplets likely partially dissolve the polycrystalline materials due to the sudden decrease in polymer concentration. The recurring introduction of solvent droplets may lead to an "annealing process" in which only a few grains of greater perfection survive and continue to grow inward.[13,32,33,35] WH analysis shows decreasing crystalline perfection closer to the center of the dish, suggesting that the crystal quality may be diminished by the droplet perturbations.

To account for the preferred out-of-plane growth orientation, we need to consider possible directors such as a mechanical field created by, for instance, a surface tension gradient between the pure toluene droplets and a concentrated polymer solution. The observed out-of-plane [211] orientation of the gyroid is consistent with lamellar sheets oriented perpendicular to the shear velocity gradient direction for surface tension induced flow. Such a configuration would be the lowest energy configuration in polymers with significant viscoelastic differences between the polymer blocks and large amplitude fields.[12,39] If the out-of-plane orientation is due to shear flow, it is unclear if it is a consequence of shear-oriented lamellae followed by an order–order transition to gyroid or if the gyroid structure appears early during structure formation and is directly oriented by the shear flow. Regardless of the kinetic pathway, there is substantial precedent for double gyroid structures as the thermodynamic morphology of copolymer and terpolymer systems with large molar mass and similar block compositions.[25,40–42] Finally, while this discussion may provide some insights into possible mechanistic details, more experimental evidence is clearly needed in order to establish the exact mechanism responsible for the observed behavior.

To establish a proof-of-principle structure–property relationship for these mesoscale bulk single crystals, we demonstrated how the local mesoscale structure translates to macroscopic responses in the form of mechanical properties. We observed that fracture characteristics change as mesostructured domains become macroscopic in size. Polycrystalline and single crystalline domains were cut from an ISA71-derived nanocomposite film with a razor blade and converted to mesoporous nonoxide ceramics with mesoporous double gyroid channels by pyrolysis.[25,43] Samples were then fractured and examined by polarized optical microscopy (POM) and scanning electron microscopy (SEM, **Figure 4**). POM revealed birefringent grains—likely from pyrolysis-induced stress—making polycrystalline (Figure 4a) and single crystalline samples (Figure 4b) easily distinguishable. When these different materials were cleaved with a diamond scribe, polycrystalline sections frequently fractured into more than two pieces with rough edges (Figure 4a, right) while single crystals cleaved consistently along flat facets (Figure 4b, right; Figure S5, Supporting Information).

Figure 4c shows an SEM image of a 1.15 mm wide single crystal fracture surface with a flat cross-section. Higher magnification revealed the characteristic "double wavy" pattern associated with the gyroid {211} plane family[43–45] (Figure 4d–f) across the entire surface. We calculated a 30% change in pore volume for thin cross-sections orthogonal to the [211] direction (Figure 4g). That is, the "double wavy" cross-section (Figure 4i) has 50% pore volume, while a dense cross-section (Figure 4h) exists $\pm 1/2$ d_{211} spacing away with only 20% pore volume, the largest difference in pore volume along any direction (Figure S6, Supporting Information). This difference in density renders {211}-type planes the preferred fracture surfaces in porous polycrystalline double gyroids.[25,43] The proximity of all 12 preferred {211} fracture planes is depicted by a single crystal gyroid mesostructure (Figure 4j) bounded by {211} planes. Groups of three different {211} planes are separated by as few as 33.6°. The consistency of one {211} plane across the entire monolith can be understood by macroscopic single-crystal-like fracture along a preferred mesoscale cleavage plane.

Finally, to demonstrate the generalizability of this single crystal growth method, we investigated both the role of substrate (see the Experimental Section and Figure S7, Supporting Information) and additional block copolymer self-assembling systems, i.e., neat ISA71 and a 33 kg mol^{-1} poly(isoprene)-*b*-poly(styrene)-*b*-poly(ethylene oxide), or ISO33, with block volume fractions I, S, and O: 30, 55, and 15 vol%, respectively. Changing the substrate from hydrophobic Teflon to a hydrophilic air-plasma treated Kapton substrate did not significantly change crystal size, shape, or orientation (Figure S7, Supporting Information). Additional polymer structures and their block volume fractions are compared in **Figure 5**a,b. Macroscopic thick films of these self-assembled polymers had similar features to those described above consisting of elongated regions (see Figure 5c,d for neat ISA71) that displayed SAXS patterns as measured on a lab source X-ray setup (beam size ≈1 mm^2) consistent with macroscopic bulk single crystals. Representative diffraction patterns are shown along a 5 mm grain in Figure 5e–h. Indexed patterns in Figure 5e,g are consistent with either a single gyroid (space group Q^{214}, $I4_132$ lattice) or a compressed double gyroid. Neat ISO33 also produced single crystal diffraction patterns consistent with the single gyroid lattice (Figure 5i). These data are consistent with the single gyroid structure observed at these ISO volume fractions published elsewhere.[40,44]

In summary, the introduction of a watch glass to facilitate the recirculation of solvent during evaporation induced self-assembly of thick films (>100 μm) of block copolymer nanocomposites yields macroscopic single crystal grains that can be identified by eye. Nanocomposites consisting of a block copolymer and preceramic polymer show consistent uniaxial orientation in the film normal direction, as revealed by SAXS orientation maps. Macroscopic single crystalline regions can be physically isolated and converted to mesoporous ceramics that fracture as single crystals along mesoscale cleavage planes over macroscopic distances. Finally, the solvent evaporation method explored here appears robust, generating mesophase bulk single crystals on different substrates and from different block copolymer chemistries, compositions, molar masses, and structures. We expect these mesophase single crystals, and the ease with which they

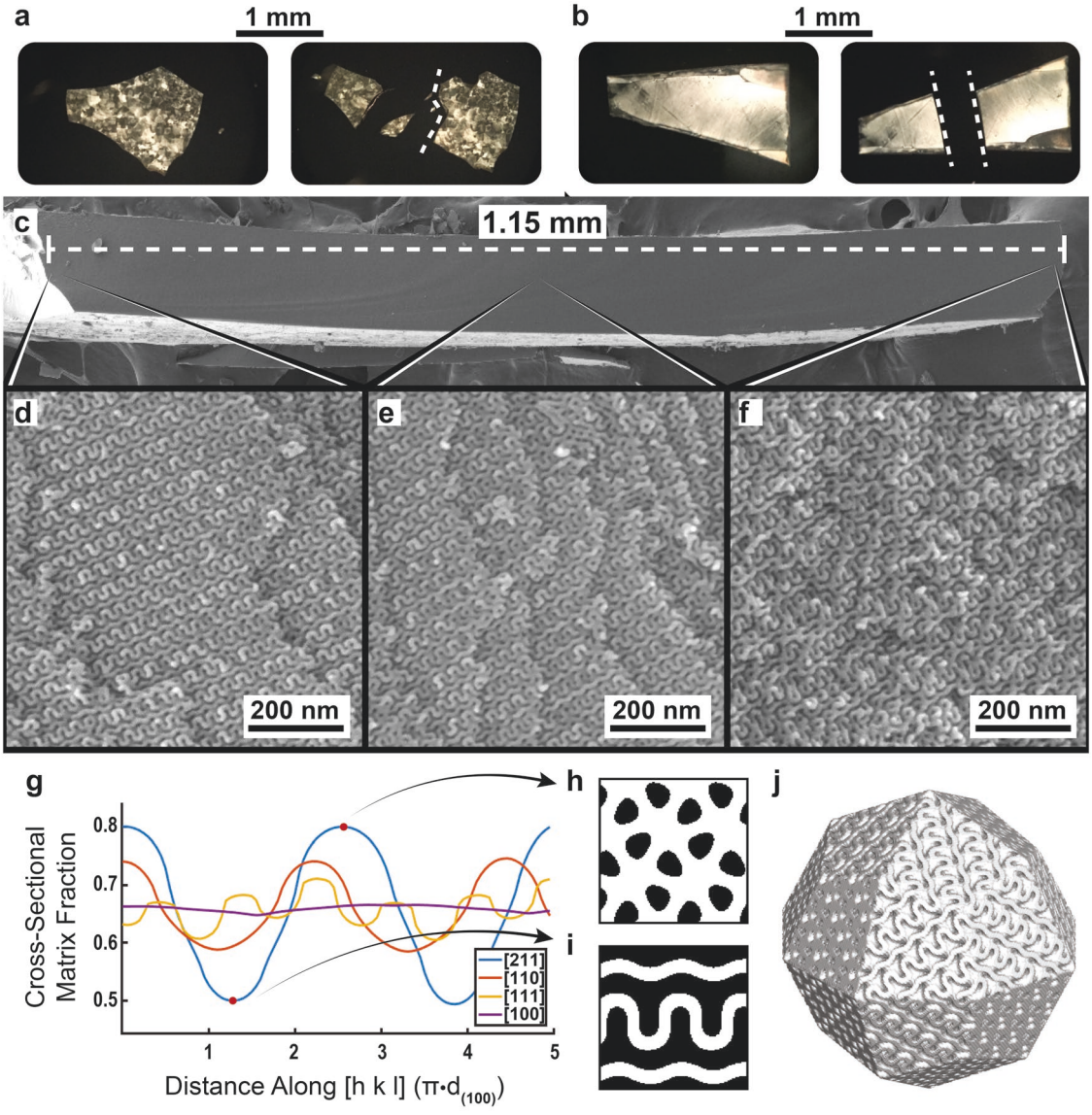

Figure 4. Microanalysis of fracture in ISA71-derived double gyroid mesoporous ceramics of varying crystallinity. a,b) Low-magnification polarized optical microscopy reveals grain structure in polycrystalline (a) and single crystalline (b) mesophase ceramics through birefringence (see Figure S5 in the Supporting Information). Dashed lines in (a,b) highlight fractured surfaces of polycrystalline (a) and single crystalline (b) monoliths. c) Low magnification SEM image of a cleaved cross-section of a single crystalline mesoporous ceramic gyroid. d–f) Characteristic {211} "double wavy" surface patterns observed over the entire length of the cross-section with changing angle as macroscopic sample bends. g) Calculated cross-sectional density fluctuations for the (211) surface (blue) as compared with other facets. h,i) There is a 30% density change between high density (h) and low density (i), "double wavy," planes along the [211] direction corresponding to marked locations in (g). j) A porous double gyroid crystal bounded by the intersections of the {211}-family of planes forming a 24-sided polyhedron.

can be prepared, to provide a platform for the discovery of mesostructure-based emergent properties and phenomena.

Experimental Section

Materials: All chemicals for polymer synthesis were purchased from Sigma-Aldrich unless otherwise stated. Poly(methyl-vinyl-silazane), trade name Durazane 1800 (PMVS), was donated by Greg McCraw from AZ Electronic Materials. Teflon evaporation dishes were acquired from VWR, catalog #89026-090. Kapton tape used as an alternate substrate (vs Teflon) was acquired from Grainger, part number 15C525.

Polymer Synthesis: Poly(isoprene)-*b*-poly(styrene)-*b*-poly(dimethylaminoethylmethacrylate), PI-*b*-PS-*b*-PDMAEMA or simply ISA, polymers were synthesized by anionic polymerization using standard Schlenk line techniques. Sec-butyl lithium (1.7 M) was used as an initiator in 200 mL of dry benzene. Sec-butyl lithium (0.18 mL for the 96 kg mol^{-1} polymer; 0.34 mL for the 71 kg mol^{-1} polymer) was added to each reactor and allowed to sit for 30 min while stirring. This time allowed for the sec-butyl lithium to clean any impurities from the reactors before polymerization was initiated. Isoprene was distilled over *n*-butyl lithium and added to the reactor: 3.07 g for 96 kg mol^{-1} ISA and 3.58 g for 71 kg mol^{-1} ISA. After 24 h, styrene was distilled over di-*n*-butyl-magnesium and added to the reactor: 5.17 g for 96 kg mol^{-1} ISA and 6.34 g for 71 kg mol^{-1} ISA. After an additional 24 h, a small amount (0.06 or 0.04 mL) of

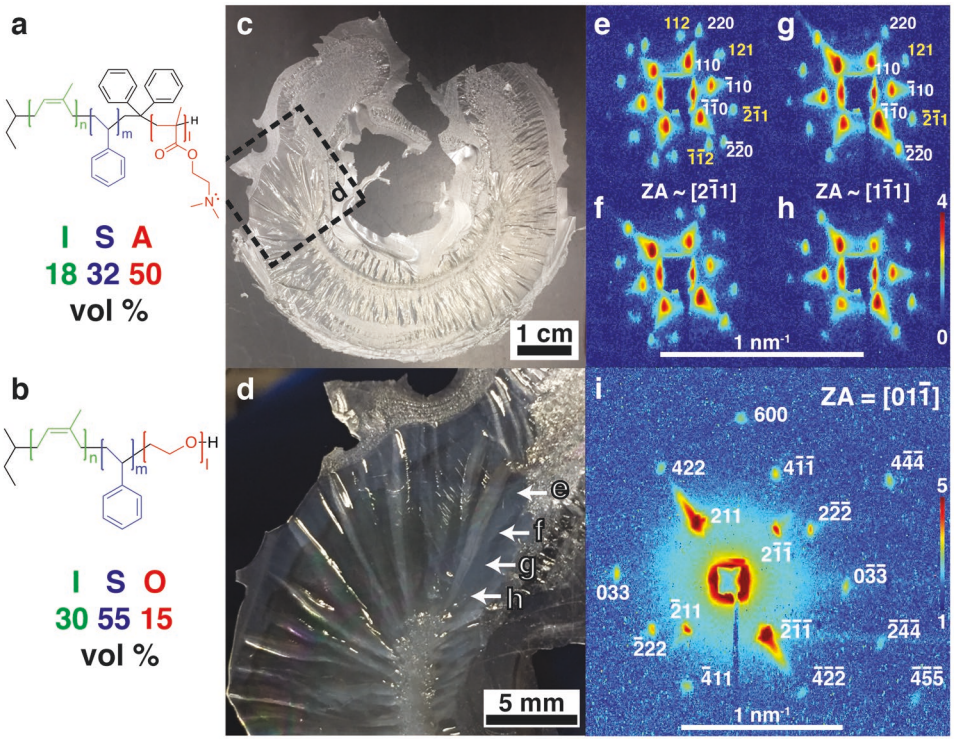

Figure 5. Mesophase bulk single crystals of neat triblock terpolymers: 71 kg mol^{-1} ISA and 33 kg mol^{-1} ISO. a,b) Structures and volume fractions of block copolymers. c,d) Macroscopic images of self-assembled film of ISA exhibiting large macroscopically identifiable grains. e–h) Single crystal diffraction patterns along a 5 mm ISA grain as indicated in (d). For lattice assignment, see text. Along the 5 mm length, the crystal tilts from zone axis of [2$\bar{1}$1] in (e) toward [1$\bar{1}$1] in (h). i) Single crystal diffraction pattern from self-assembled ISO film consistent with single gyroid lattice oriented along the [01$\bar{1}$] zone axis. 2D SAXS patterns are log color scale.

diphenyl ethylene (distilled from *n*-butyl lithium) was added to the reactor to end-cap the PI-*b*-PS diblock copolymers. A solvent swap to dry (once distilled) tetrahydrofuran was performed and dimethylamino ethylmethacrylate (distilled from tri-ethyl aluminum) was added to the reactor at −40 °C using an isopropyl alcohol/ethylene glycol/dry ice bath. The reaction continued for 1 h before termination with degassed methanol. Gel permeation chromatography (GPC) was used to determine the molar mass of a poly(isoprene) aliquot removed before styrene addition. H^1-nuclear magnetic resonance (NMR) spectroscopy was used to determine the molar ratio of PI:PS:PDMAEMA. The two polymers and their stoichiometry used in this study were 96 kg mol^{-1} ($I_{226}S_{284}A_{324}$) and 71 kg mol^{-1} ($I_{159}S_{209}A_{247}$). Using densities for I/S/A of 0.92/1.047/1.18 g cm^{-3} yielded polymers with volume fractions: 19/32/49 vol% for 96 kg mol^{-1} ISA and 18/32/50 vol % for 71 kg mol^{-1}. Both had total polydispersity indices of 1.09 by GPC using PS standards.

Poly(isoprene)-*b*-poly(styrene)-*b*-poly(ethylene oxide), PI-*b*-PS-*b*-PEO or simply ISO, was synthesized using anionic chemistry, similar to above, described elsewhere.[46]

Evaporation-Induced Self-Assembly: A 22 mL solution containing 5 wt% self-assembling polymer blend in toluene was prepared by adding 0.617 g ISA and 4 mg dicumyl peroxide in a 20 mL, Teflon-capped, scintillation vial. The vial was then transferred into a glovebox for the addition of 0.432 g PMVS and dry toluene stored over molecular sieves (Alfa Aesar). Solutions were also prepared with double these quantities and then later divided into two separate evaporation dishes.

After solutions were thoroughly homogenized, they were poured into 7.5 cm diameter Teflon dishes with 1 inch walls (VWR catalog #89026-090). The Teflon evaporation dishes were preheated to 50 or 35 °C (for 96 or 71 kg mol^{-1} ISA solutions, respectively) on a hot plate in a box continuously purged with nitrogen (4 L h^{-1}). A 100 mm diameter watch glass was positioned as a lid, convex side pointed downward, and a hemispherical dome (cut from half of a 500 mL round-bottom flask) positioned over both watch glass and dish to further slow evaporation. When toluene droplets were no longer observed on the watch glass, the temperature was increased to 130 °C for 3 h to induce PMVS crosslinking before cooling to room temperature. Films were mechanically robust and could be easily removed from evaporation dish without inducing strain.

The evaporation of neat ISA and ISO was performed by making a 5 wt% solution of each polymer in dry toluene. For neat ISA, identical drying conditions described above were used; only the evaporation lasted 25 days. For neat ISO, a 5 cm diameter dish with 1 inch wall height was placed on a heating plate at 50 °C under a 75 mm watch glass lid (convex side down) and glass dome. Evaporation occurred over 10 days, at which point no liquid was observed to remain in the dish. The dish was then placed into a vacuum oven at 50 °C for 12 h, yielding a brittle film that shattered upon removal from dish.

Pyrolysis: Hybrid ISA/PMVS films were pyrolyzed to 1100 °C in ammonia (electronic grade, 99.9995% from Praxair) with a 4 L h^{-1} flow rate in a flow-through tube furnace (Lindberg model 55035). Hybrid films were fractured after being immersed in liquid nitrogen in order to limit mechanical deformation. Single crystal regions were isolated prior to pyrolysis by cutting the fractured pieces with a razor blade for studies with polarized optical microscopy. Samples were placed in a boron nitride (BN) crucible machined from a 3 inch long, 0.75 inch diameter, BN dowel (McMaster Carr) to have a 1.5 mm wide slit along the dowel length. Films were placed in the slit to prevent uneven deformation (curling) during pyrolysis such that postpyrolysis materials were mostly planar, retaining their prepyrolysis shape. The furnace schedule was 2 °C h^{-1} to 1100 °C, 1100 °C for 3 h, followed by passive cooling to room temperature before the flow-through furnace was purged with nitrogen and samples could be safely removed.

Supporting Information

Supporting Information is available from the Wiley Online Library or from the author.

Acknowledgements

The authors thank Gil Toombes for conversations and Greg McCraw of AZ Electronic Materials for donation of polysilazane (Durazane 1800). Work by L.A.E. and U.B.W. was supported by the U.S. Department of Energy (DOE), Basic Energy Sciences (BES) under award DE-SC0010560. Work by S.M.G. was supported by the U.S. DOE, BES under award DE-SC0017631. P.A.B. was supported by the NSF Graduate Research Fellowship Program (DGE-1650441). R.P.T. was supported by the NSF single investigator grant to U.W. (DMR-1707836). The work made use of Cornell High Energy Synchrotron Source (CHESS) supported by the NSF (DMR-1332208), as well as of the Cornell Center for Materials Research Shared Facilities which are supported through the NSF MRSEC program (DMR-1719875).

Conflict of Interest

The authors declare no conflict of interest.

Keywords

block copolymer self-assembly, mesoscale single crystals, self-assembly, X-ray structure

Received: April 22, 2019
Revised: July 17, 2019
Published online:

[1] Z.-R. Chen, J. A. Kornfield, S. D. Smith, J. T. Grothaus, M. M. Satkowski, *Science* **1997**, *277*, 1248.
[2] S. O. Kim, H. H. Solak, M. P. Stoykovich, N. J. Ferrier, J. J. de Pablo, P. F. Nealey, *Nature* **2003**, *424*, 411.
[3] F. S. Bates, G. H. Fredrickson, *Phys. Today* **1999**, *52*, 32.
[4] F. S. Bates, M. A. Hillmyer, T. P. Lodge, C. M. Bates, K. T. Delaney, G. H. Fredrickson, *Science* **2012**, *336*, 434.
[5] A. Keller, E. Pedemonte, F. M. Willmouth, *Nature* **1970**, *225*, 538.
[6] J. Y. Cheng, A. M. Mayes, C. A. Ross, *Nat. Mater.* **2004**, *3*, 823.
[7] C. De Rosa, C. Park, E. L. Thomas, B. Lotz, *Nature* **2000**, *405*, 433.
[8] T. L. Morkved, M. Lu, A. M. Urbas, E. E. Ehrichs, H. M. Jaeger, P. Mansky, T. P. Russell, *Science* **1996**, *273*, 931.
[9] T. Thurn-Albrecht, J. Schotter, G. A. Kästle, N. Emley, T. Shibauchi, L. Krusin-Elbaum, K. Guarini, C. T. Black, M. T. Tuominen, T. P. Russell, *Science* **2000**, *290*, 2126.
[10] C. Bates, T. Seshimo, M. J. Maher, W. J. Durand, J. D. Cushen, L. M. Dean, G. Blachut, C. J. Ellison, C. G. Wilson, *Science* **2012**, *338*, 775.
[11] S. Park, Y. Kim, W. Lee, S.-M. Hur, D. Y. Ryu, *Macromolecules* **2017**, *50*, 5033.
[12] S. S. Patel, R. G. Larson, K. I. Winey, H. Watanabe, *Macromolecules* **1995**, *28*, 4313.
[13] J. Bodycomb, Y. Funaki, K. Kimishima, T. Hashimoto, *Macromolecules* **1999**, *32*, 2075.
[14] B. J. Dair, A. Avgeropoulos, N. Hadjichristidis, M. Capel, E. L. Thomas, *Polymer* **2000**, *41*, 6231.
[15] K. Hur, Y. Francescato, V. Giannini, S. A. Maier, R. G. Hennig, U. Wiesner, *Angew. Chem., Int. Ed.* **2011**, *50*, 11985.
[16] M. Fruchart, S.-Y. Jeon, K. Hur, V. Cheianov, U. Wiesner, V. Vitelli, *Proc. Natl. Acad. Sci. USA* **2018**, *115*, E3655.
[17] L. Lu, Z. Wang, D. Ye, L. Ran, L. Fu, J. D. Joannopoulos, M. Soljacic, *Science* **2015**, *349*, 622.
[18] S. W. Robbins, P. A. Beaucage, H. Sai, K. W. Tan, J. G. Werner, J. P. Sethna, F. J. DiSalvo, S. M. Gruner, R. B. Van Dover, U. Wiesner, *Sci. Adv.* **2016**, *2*, e1501119.
[19] K. Hur, R. G. Hennig, U. Wiesner, *J. Phys. Chem. C* **2017**, *121*, 22347.
[20] G. E. S. Toombes, A. C. Finnefrock, M. W. Tate, R. Ulrich, U. Wiesner, S. M. Gruner, *Macromolecules* **2007**, *40*, 8974.
[21] A. C. Finnefrock, R. Ulrich, G. E. S. Toombes, S. M. Gruner, U. Wiesner, *J. Am. Chem. Soc.* **2003**, *125*, 13084.
[22] A. C. Finnefrock, R. Ulrich, A. Du Chesne, C. C. Honeker, K. Schumacher, K. K. Unger, S. M. Gruner, U. Wiesner, *Angew. Chem.* **2001**, *113*, 1247.
[23] R. Dehmel, J. A. Dolan, Y. Gu, U. Wiesner, T. D. Wilkinson, J. J. Baumberg, U. Steiner, B. D. Wilts, I. Gunkel, *Macromolecules* **2017**, *50*, 6255.
[24] M. Kamperman, C. B. W. Garcia, P. Du, H. Ow, U. Wiesner, *J. Am. Chem. Soc.* **2004**, *126*, 14708.
[25] E. Susca, P. A. Beaucage, M. A. Hanson, U. Werner-Zwanziger, J. W. Zwanziger, L. A. Estroff, U. Wiesner, *Chem. Mater.* **2016**, *28*, 2131.
[26] E. J. W. Crossland, M. Kamperman, M. Nedelcu, C. Ducati, U. Wiesner, D.-M. Smilgies, G. E. S. Toombes, M. A. Hillmyer, S. Ludwigs, U. Steiner, H. J. Snaith, *Nano Lett.* **2009**, *9*, 2807.
[27] A. S. Finnemore, M. R. J. Scherer, R. Langford, S. Mahajan, S. Ludwigs, F. C. Meldrum, U. Steiner, *Adv. Mater.* **2009**, *21*, 3928.
[28] M. R. J. Scherer, P. M. S. Cunha, U. Steiner, *Adv. Mater.* **2014**, *26*, 2403.
[29] D. A. Hajduk, P. E. Harper, S. M. Gruner, C. C. Honeker, G. Kim, E. L. Thomas, L. J. Fetters, *Macromolecules* **1994**, *27*, 4063.
[30] G. K. Williamson, W. H. Hall, *Acta Metall.* **1953**, *1*, 22.
[31] E. A. Sulyanova, A. Shabalin, A. V. Zozulya, J.-M. Meijer, D. Dzhigaev, O. Gorobtsov, R. P. Kurta, S. Lazarev, U. Lorenz, A. Singer, O. Yefanov, I. Zaluzhnyy, U. Besedin, M. Sprung, A. V. Petukhov, I. A. Vartanyants, *Langmuir* **2015**, *31*, 5274.
[32] C. Tang, A. Tracz, M. Kruk, R. Zhang, D.-M. Smilgies, K. Matyjaszewski, T. Kowaleswski, *J. Am. Chem. Soc.* **2005**, *127*, 6918.
[33] D. E. Angelescu, J. H. Waller, D. H. Adamson, R. A. Register, P. M. Chaikin, *Adv. Mater.* **2007**, *19*, 2687.
[34] C. O. Osuji, *Macromolecules* **2010**, *43*, 3132.
[35] J. E. Seppala, R. L. Lewis, T. H. Epps, *ACS Nano* **2012**, *6*, 9855.
[36] M. Kimura, M. J. Misner, T. Xu, S. H. Kim, T. P. Russell, *Langmuir* **2003**, *19*, 9910.
[37] J. Hwang, J. Huh, B. Jung, J.-M. Hong, M. Park, C. Park, *Polymer* **2005**, *46*, 9133.
[38] W. Zhao, Y. Zhang, X. Wang, X. Hu, F. Liu, T. P. Russell, G. Zhou, *J. Polym. Sci., Part B: Polym. Phys.* **2018**, *56*, 1369.
[39] U. Wiesner, *Macromol. Chem. Phys.* **1997**, *198*, 3319.
[40] T. H. Epps, E. W. Cochran, T. S. Bailey, R. S. Waletzko, C. M. Hardy, F. S. Bates, *Macromolecules* **2004**, *37*, 8325.
[41] A. J. Meuler, M. A. Hillmyer, F. S. Bates, *Macromolecules* **2009**, *42*, 7221.
[42] S. Park, Y. Kim, H. Ahn, J. H. Kim, P. J. Yoo, D. Y. Ryu, *Sci. Rep.* **2016**, *6*, srep36326.
[43] T. Hashimoto, Y. Nishikawa, K. Tsutsumi, *Macromolecules* **2007**, *40*, 1066.
[44] J. G. Werner, T. N. Hoheisel, U. Wiesner, *ACS Nano* **2014**, *8*, 731.
[45] M. She, T. Lo, R. Ho, *Macromolecules* **2014**, *47*, 175.
[46] T. S. Bailey, C. M. Hardy, T. H. Epps, F. S. Bates, *Macromolecules* **2002**, *35*, 7007.